An unprecedented oxidised julolidine-BODIPY conjugate and its application in real-time ratiometric fluorescence sensing of sulfite

D. Sirbu[a*], L. Zeng[a], P. G. Waddell[b] and A. C. Benniston[a*]

Reaction of a julolidine-based BODIPY compound with silver (I) ions in the presence of white light produced the oxidised julolidine version (**OXJUL**) containing a quaternary nitrogen. The oxidation of one ring at the julolidine site is highly unusual and there is no other reported literature example. The fluorescence maximiun of **OXJUL** is altered from 648 nm to 608 nm by the addition of an aqeuous solution of Na_2SO_3 over several minutes. In the presence of a large excess of sulfite a further slower reaction is observed which further shifts the emission maximum to 544 nm. The alterations form the basis of a real-time ratiometric sensor for sulfite and its detection in a white wine.

Introduction

The selective detection of analytes is critical in many branches of science, especially where their concentration is low and can have detrimental effects.[1] The clear case is poisonous metal ions (*e.g.,* Hg^{2+}) that can be sequestered by peptides and shut down essential biological processes.[2] Many different methods have been developed to detect analytes in their natural environments including electrochemical,[3] spectroscopic[4] and titrimetric;[5] all the methods have their advantages and disadvantages and there is no one unique solution for analyte detection. Over the past several years the selective monitoring of anions has become important especially phosphate,[6] halides,[7] nitrate,[8] cyanide,[9] carbonate[10] and acetate.[11] The anion sulfite is especially relevant as it is an anti-oxidant and used extensively as a preservative in the food industry.[12] Several groups have developed methods for sulfite recognition[13] especially detection based on fluorescence monitoring.[14] The operation of many systems depends on the addition of a sulfite anion to a double-bond in a conjugated chromophore. Perturbation of the structure in many examples results in colour changes that are readily monitored in real-time.

During studies into the coordination chemistry of the pyridine-based BODIPY derivative, **JUL**, it was noticed that an interesting photochemical reaction occurred in the presence of Ag^+ ions. The electron donating julolidine subunit was transformed to the unprecedented oxidised version containing the quaternized nitrogen (**OXJUL**). There was no indication in the literature for such a reaction at a julolidine unit; the oxidation product is usually a dimer which cannot occur in **JUL** as the para position is blocked.[15] Given the presence of the iminium ion it was speculated that addition of a nucleophile such as sulfite might occur, and result in an alteration in the observed fluorescence. In both aqueous and ethanol/water solutions a very distinct fluorescence response was observed, which was monitored by a ratiometric method. The protocol was robust enough to measure directly the sulfite concentration in a white wine. Unlike many other fluorescence-based sulfite detectors the dye has a second response so that long-term exposure to sulfite can be monitored too.

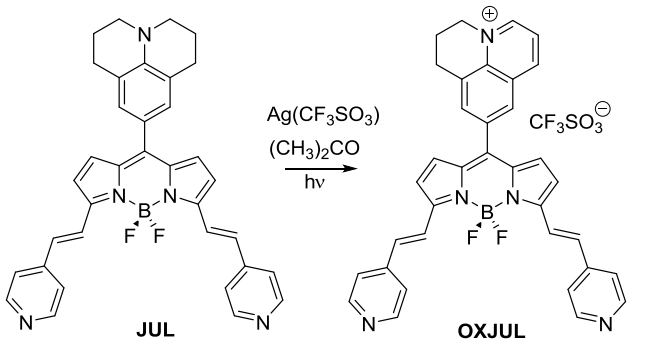

Scheme 1. Procedure used in the preparation of the oxidised julolidine-based BODIPY derivative **OXJUL**.

Results and discussion

Synthesis

The preparation of compound **JUL** followed a modified method as described previously.[16] In an endeavour to monitor coordination of silver ions to **JUL** excess silver triflate was added to a DMSO-d_6 solution and a ^{1}H NMR spectrum recorded. An immediate upfield shift of certain resonances was observed especially those associated with protons 2 of the pyridyl units; smaller shifts were also seen for the alkene resonances. The evidence is supportive of interaction of Ag^+ ions with **JUL** probably via the pyridyl nitrogen. More interestingly when the solution was left under white light further changes in the ^{1}H NMR spectrum occurred over time. No changes in the ^{1}H NMR spectrum transpired if the mixture was kept in the dark, suggesting that the reaction was photodriven. The formation of the Ag^+ complex with **JUL** is critical for driving the photochemical reaction. It was also noted that the photochemical reaction was highly solvent dependent, taking place faster in solvents such as acetonitrile or acetone.

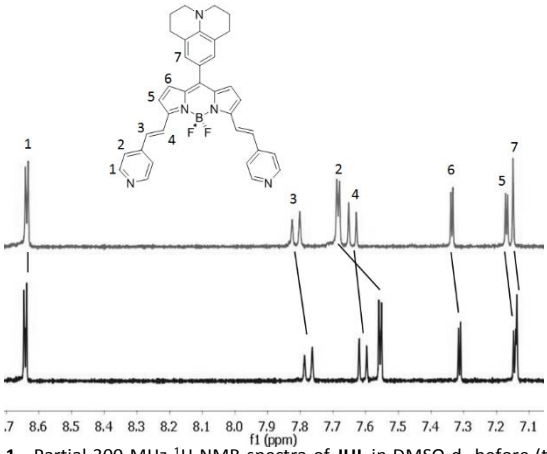

Figure 1. Partial 300 MHz ^{1}H NMR spectra of **JUL** in DMSO-d_6 before (top) and after addition of silver triflate (bottom).

Based on the NMR findings a scale-up reaction was undertaken in which **JUL** was irradiated in acetone, and the reaction was monitored by tlc. After *ca.* 7-10 days a coloured solid was obtained which required no further purification. The positive ion ESI mass spectrum of the product contained a clear ion at m/z = 566 which is three hydrogens less than the starting material. Such an oxidation is consistent with the formation of a quinolinium cation, and was verified by a single-crystal X-ray diffraction determination.

X-ray Crystallography

Crystals suitable for analysis were grown by slow diffusion of aqueous sodium *p*-toluenesulfonate (NaOTs) into a solution of **OXJUL** in DMSO. The isolated compound crystallised in the centrosymmetric, triclinic space group *P-1*. The asymmetric unit comprises two **OXJUL** cations, two TsO^- anions and ten water molecules, three of which were modelled as disordered over two positions. The molecular structure of **OXJUL** is illustrated in Figure 2, and selected bond lengths and angles are shown in Table 1. As there are two crystallographically independent equivalents of each ion all geometric parameters are presented as averages of the two equivalent values.

The two *trans* C = C bonds of the pyridylethylene moiety (average bond length *ca.* 1.34 Å) are confirmed by the X-ray analysis. Within the julolidine fragment the imine bond (N = C_{JUL} average bond length *ca.* 1.32 Å) along with the *cis* C = C bond (C = C_{JUL} average bond length *ca.* 1.37 Å) confirm the oxidation of the julolidine moiety to form a quinolinium cation. No other crystal structure was found in the Cambridge Crystallographic Database for a C–N oxidised julolidine fragment. The closest analogues to **OXJUL** are the benzoquinolinones, although in their ketonic form the nitrogen atom is not quaternized. As observed in previous *meso*-julolidine BODIPY structures, the oxidised julolidine subunit is twisted with respect to the boron dipyrromethene core (torsion angle *ca.* 46°). The two cations are arranged in such a way that the vinyl-pyridine fragments form off-set anti-parallel π···π interactions to either the pyrrole or the central BODIPY heterocycle of an adjacent cation (distances between the ring centroids *ca.* 3.6 and 3.8 Å).

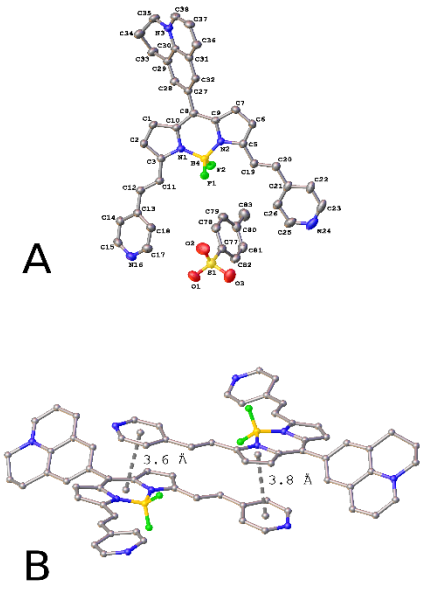

Figure 2. Structure of one of the independent cation-anion pairs of **OXJUL** (**A**) with ellipsoids drawn at the 50% probability level. Water molecules and hydrogen atoms have been omitted for clarity. A second view highlighting the intermolecular π···π interactions (**B**) has also been included.

In each of the two independent cations the two pyridyl subunits are out-of-plane with respect to the BODIPY core to varying degrees; the interplanar angles between the pyridyl rings and the BODIPY core range from *ca.* 5-22°. As the DFT modelling returns a mostly planar structure these conformational variations can be attributed to solid state intermolecular interactions such as the π···π interactions described above.

Table 1. Selected bond lengths and angles for **OXJUL.**

Atoms	Bond Length / Å (Experimental[a] / Calculated[b])	Atoms or Planes	Angle / ° (Experimental[a] / Calculated[b])
B – F	1.391 / 1.408	F – B – F	108.78 / 108.91
N – B	1.545 / 1.548	N – B – N	106.96 / 107.38
C = C_{trans}	1.339 / 1.350	Py – BD	4.9, 12.4, 22.0, 30.2
C = C_{JUL}	1.370 / 1.371	BD' – BD''	2.8
N = C_{JUL}	1.320 / 1.328	^{ox}JUL – BD	46.0 / 60.8

[a]Values represent the average of the bond lengths and angles of the two cations in the asymmetric unit. [b] Values calculated using DFT (B3PW91) and the 6-311+G(d, p) basis set in the gas phase.

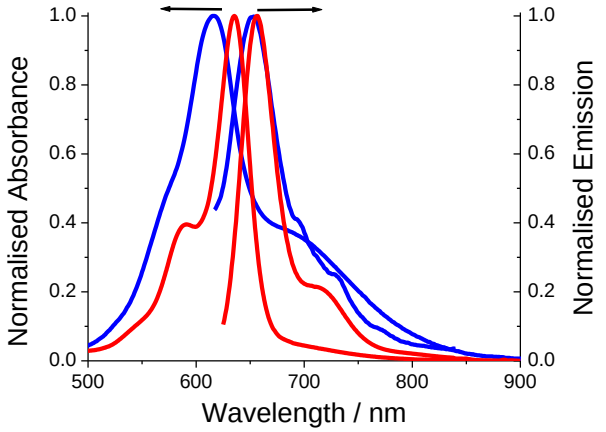

Figure 3. The room temperature absorption and emission spectra of **JUL** (blue) and **OXJUL** (red) in DMSO.

Absorption and fluorescence

Room temperature electronic absorption spectra for **JUL** and **OXJUL** in DMSO are shown in Figure 3, with relevant parameters presented in Table 2. The absorption spectrum for **JUL** shows typical BODIPY-based π–π* transitions at λ_{max} = 616 nm, and a pronounced broad absorption centred at λ_{max} = 661 nm. Based on previous work[16,17] this band is associated with a charge-transfer (CT) transition involving electron donation from the julolidine group to the BODIPY core. Whereas the localised BODIPY-based transition is higher in energy than the CT band for **JUL** the situation changes completely when the julolidine group is oxidised. The clear broad CT transition for **OXJUL** is removed and the BODIPY-based absorption profile is red-shifted, λ_{max} = 636 nm. A small tail is also observed to the low-energy region which can be fitted to a broad Gaussian profile (see ESI).

The room temperature fluorescence spectra for **JUL** and **OXJUL** in DMSO are shown in Figure 3, with relevant parameters presented in Table 2. The emission spectrum for **JUL** consists of a main band localised at λ_{EM} = 656 nm with a smaller broad band on the low-energy side. The Stokes shift (SS) of 919 cm^{-1} is consistent with previous known values for similar compounds, and the fluorescence quantum yield (ϕ_{FLU}) is 1.0 %. In comparison the ϕ_{FLU} for **OXJUL** of 67% is significantly greater, and consistent with removal of the deactivating and non-fluorescent CT state. The SS is reduced when compared to **JUL**, and more consistent to values found for BODIPYs.[18]

Table 2. Room temperature UV-Vis-NIR absorption and emission parameters for **JUL** and **OXJUL** in DMSO.

Compound	λ_{abs} / nm	λ_{abs} [a] / nm	λ_{em} / nm	Stokes' shift SS / cm^{-1}	Φ_f [b] / %
JUL	340, 570 sh, 616, 690 sh	552, 578, 616, 661[c]	653, 696 sh, 732 sh	919	1.0±0.2
OXJUL	344, 589 sh, 636	562, 591, 610[c] 636	656, 715 sh	479	67±0.1

[a]Data obtained by deconvolution of the absorption spectra. [b]Quantum yields were calculated relative to H_2TPP in toluene under N_2 (Φ_f = 11 %) and aza-BODIPY in methanol (Φ_f = 33 %).[19] [c]The CT absorption band. [d]The Stokes shift calculated versus deconvoluted BODIPY absorption band.

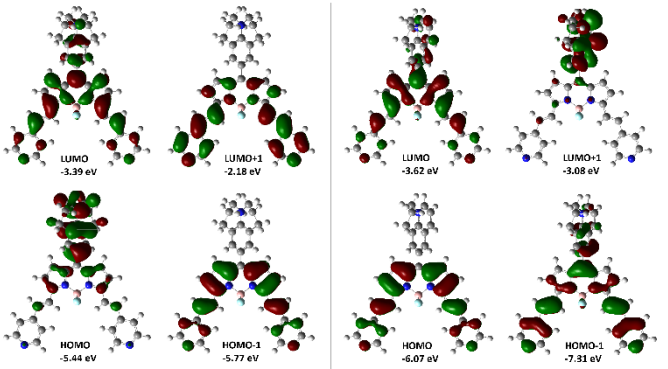

Figure 4. Representation of the Gaussian calculated Kohn-Sham frontier molecular orbitals for **JUL** (left) and **OXJUL** (right) in DMSO solvent using IEF-PCM model at a B3PW91/6-311+G(d,p) theoretical level.

Molecular modelling

In an attempt to understand the nature of the electronic transitions within the BODIPY compounds, density functional theory (DFT) calculations (B3PW91, 6-311+G(d,p)) were performed and optimized geometries computed for **JUL** and **OXJUL**. The calculated Kohn-Sham frontier molecular orbitals (MO) for **JUL** and **OXJUL** are presented in Figure 4, and the diagram of MO energies is presented in Supporting Information. For compound **JUL** the HOMO-1 is localised on the vinylpyridyl-BODIPY unit and the HOMO is predominantly localised on the julolidine moiety. The LUMO is mainly associated with the vinylpyridyl-BODIPY core, so very crudely the HOMO→LUMO electronic transition represents julolidine to vinylpyridyl extended BODIPY charge transfer. The calculated HOMO to HOMO-1 energy gap is only 0.33 eV in line with the experimental observation for separation of the BODIPY and CT bands. Thus it is reasonable to assume that the favourable driving force for charge separation is responsible for fluorescence quenching. Given the nature of the excited CT state, consisting of a partially oxidised julolidine group and partial negative charge localization on the vinylpyridyl units, any close Ag^+ coordination at the pyridine would pull electron

density away from the julolidine group. Any build-up of negative charge at the pyridine site would be neutralised by the presence of the cation. The reaction is light driven presumably via the excited singlet state and requires reduction of Ag^+ to metallic silver. Although no direct evidence supports this mechanism it is clear that coordination of **JUL** to Ag^+ is necessary for the light-induced reaction to occur.

Table 3. The calculated CT and BD transitions energy for **JUL** and **OXJUL** in DMSO solvent using IEF-PCM model at B3PW91/6-311+G(d,p) TD-DFT theoretical level. Values in brackets represent the experimentally determined values.

Compound name	CT transition energy / eV	BD transition energy / eV
JUL	1.82 (1.88)	2.13 (2.01)
OXJUL	2.29 (2.07)	2.03 (1.95)

In the case of **OXJUL** the HOMO, HOMO-1 and LUMO are mostly localized on the extended BODIPY core, while LUMO+1 is almost exclusively located on the quinolinium cation. Hence, the HOMO to LUMO+1 electronic transition can be considered electron transfer from the extended BODIPY to the quinolinium cation, and fully consistent with CT character. This CT state is likely well separated from the BODIPY localised excited state since the calculated LUMO to LUMO+1 energy gap is 0.54 eV. This observation also explains why the fluorescence is significantly restored upon the oxidation of julolidine moiety, since the CT state is now located higher in energy than the emissive BODIPY state.

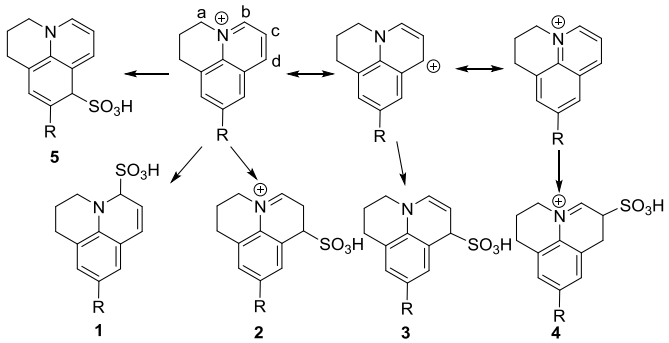

Figure 5. Potential products from sulfite addition to the oxidised julolidine unit in **OXJUL** and where R is the rest of the molecule. Note: sulfite addition reduces π-conjugation in the julolidine subunit and in **2** and **4** leaves the nitrogen quaternized.

Time-dependent (TD-DFT) calculated electronic absorption spectra are collected in Supporting Information, with the relevant parameters shown in Table 3. Although the calculated energy difference between the BODIPY and CT transitions is larger than for the experimental data, the TD-DFT predicted bathochromic shift upon oxidation of julolidine unit and interchange of the CT and BD bands energy positions fits well with the experimental data. Generally the theoretical absorption profiles match quite well with the experimental results in relation to the shift trends of the bands and the relative position of the electronic transitions.

Reaction of Sulfite with OXJUL

The sulfite anion is a recognised nucleophile which can add reversibly to certain function groups such as a carbonyl[20] and the guanidinium moiety.[21] By inspection of **OXJUL** one clear site for reaction is the oxidised julolidine where several different products are feasible (Figure 5). Calculations support that the most favoured product which leaves the nitrogen quaternized is **2** and is slightly more favoured than **4**. The derivatives **1**, **3** and **5** result in a lone-pair at the nitrogen. The alternative reactions sites are located at the BODIPY core at the meso position and vinyl group (see ESI). Reactions at these two sites would be expected to dramatically perturb the chromophore, whereas sulfite addition to the oxidised julolidine group removes a double bond and may also alter its electron withdrawing nature.

In an attempt to identify the reaction products a ^{1}H NMR spectrum of **OXJUL** in d_6-DMSO was recorded before and after the addition of an aqueous solution of Na_2SO_3. Furthermore, a dilute DMSO solution was treated with Na_2SO_3(aq) and monitored under UV excitation by eye. In the latter experiment the clear red emission was quenched, but was restored by the addition of a small amount of acid (see ESI). Very distinct alterations in the ^{1}H NMR spectrum were observed in line with a reaction at the oxidised julolidine group (see ESI). The clear resonances for protons ***a*** through ***d*** (Figure 5) disappeared and new peaks appeared at 6.5 ppm (doublet), 5.8 ppm (doublet of a doublet) and 4.8 ppm (doublet). The sulfite addition product is tentatively assigned to compound **3** (Figure 5) by comparison to a simulated ^{1}H NMR spectrum for such a compound.[22] A mass spectrum collected also confirmed formation of an adduct (see ESI). Noting that compound **3** is converted to **2** by the addition of a proton the observed fluorescence changes can be therefore easily explained. The fluorescent **OXJUL** is firstly converted to derivative **3** which switches on intramolecular charge-transfer, because the nitrogen lone-pair is reintroduced; the CT state formed establishes an efficient fluorescence quenching pathway. The CT state is then removed as the quaternized nitrogen is reformed in derivative **2**. The sulfite addition reaction in an aqueous solution should mirror closely that in DMSO except that protonation would be more probable.

Addition of sodium sulfite to a buffered aqueous solution[23] of **OXJUL** resulted in an alteration to the absorption spectrum (see ESI). The absorbance for the long-wavelength absorption profile at 628 nm decreased and a new band appeared at 574 nm. The blue-shift is consistent with perturbation of the chromophore by reaction at the oxidised julolidine site. Emission spectra (Figure 6) collected during the reaction also mirrored absorbance changes. Firstly a relatively fast reaction occurred leading to a blue-shift of *ca.* 38 nm in the emission wavelength to 608 nm. The band-shape is similar to the starting spectrum and the compound formed is still highly emissive suggesting that the oxidised julolidine moiety is not removed during the reaction. In the second stage a slower reaction occurred resulting in a stronger (64 nm relative to the intermediate species) blue-shift to 544 nm (Figure 6). This signal was stable for at least twelve hours. The two distinct segments within the fluorescence response are different to previously published

systems,[24] opening up the possibility to monitor long-term exposure of an environment to sulfite.

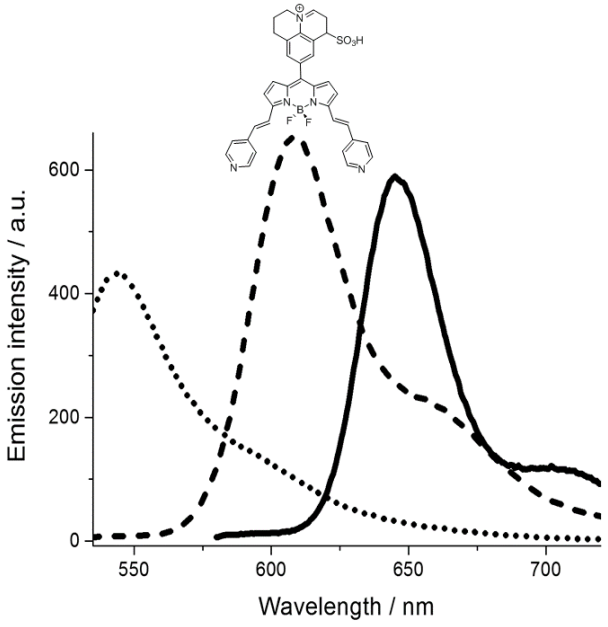

Figure 6. (a) The room temperature emission spectra of aqueous pH = 7 solution of **OXJUL** before sulfite addition (solid line, λ_{ex} = 570 nm) (b) First fast reaction upon addition of 1000 eq excess sulfite (dashed line, λ_{ex} = 525 nm). (c) Second slow process with large excess sulfite (dotted line, λ_{ex} = 525 nm). Insert shows proposed product from the first reaction.

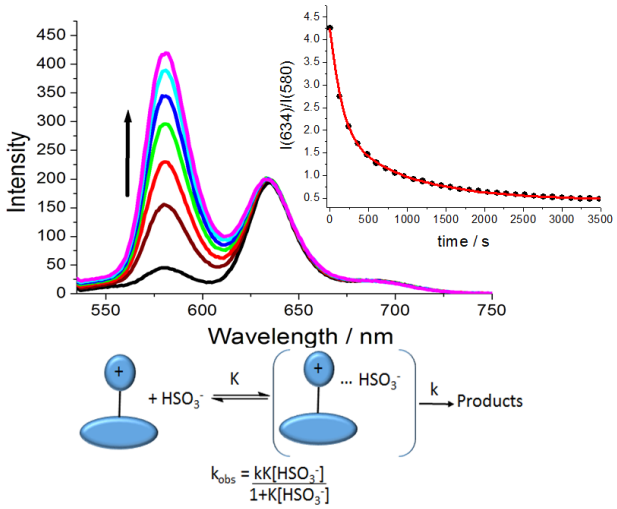

Figure 7. Top: Fluorescence profiles following the addition of **OXJUL** (conc = 0.5 μM) to an ethanol/water mixture (75:25) containing 500 equivalents of Na_2SO_3. Insert shows the ratio of the two peaks over time and a least-squares fit to a dual exponential (red line). Bottom: Pictorial representation of proposed equilibrium with **OXJUL** and the kinetic model. Note: as $K[HSO_3^-] >> 1$ the equation simplifies so that $k_{obs} = k$.

Working under pure aqueous conditions did suffer from one problem in that the dye started to precipitate from solution over *ca.* 30 mins. Since ultimately the aim was to detect sulfite in a wine sample the solution was changed to an ethanol/water (75:25) mixture. Controlled experiments were performed where a known concentration of **OXJUL** was added to Na_2SO_3 at various concentrations and the reaction monitored over time (see ESI). In a typical experiment (Figure 7) the intensity of the short wavelength band increased with respect to the long wavelength profile and the ratio (I_{634}/I_{580}) of the two maxima was monitored over time. The kinetic profile was best fit to a dual exponential decay with lifetimes of t_1= 142 s and t_2 = 900 s. The observed rate constant (k_{obs}) for the first process remains relatively constant over a range of 300-1000 equivalents of Na_2SO_3 (see ESI). A basic model[25] to explain this observation is the formation of an equilibrium complex between **OXJUL** and HSO_3^- (Figure 7) followed by a chemical reaction. At high [HSO_3^-] there is sufficient build-up of the encounter complex such that $k_{obs} = k$ which in this case is *ca.* 9 x 10^{-3} s^{-1}.

Using the full set of fluorescence response data the best working range and detection limit was determined along with a calibration plot (see ESI). Typically, the reciprocal of I(580)/I(634) values at set times were plotted versus the number of equivalents of sulfite to find the optimum sampling time and best linearity response (see ESI). At early time delays (< 5 mins) calibration plots were generally poor representing the fact that the fast first reaction dominates and a systematic error is introduced. The best sampling time was found to be between 10-20 mins up to about 2000 equivalents of sulfite. Calibration plots were linear with R^2 = 0.98 (see ESI). The limit of detection (LOD), calculated using 3σ/slope, is around 9 x 10^{-5} M. This value is limited by the rate of the first reaction which becomes slow at low equivalents of sulfite (*vide supra*).[26]

To evaluate the anion selectivity of **OXJUL**, ten other typical anions F^-, Cl^-, Br^-, I^-, SO_4^{2-}, PO_4^{3-}, NO_3^-, NO_2^-, CO_3^{2-}, CH_3COO^- were tested under identical conditions (see ESI). The nucleophilic reaction at **OXJUL** is specific to the HSO_3^- ion, triggering about a 8 times more emission ratio change than any of the other ions. This finding is encouraging for the selective detection of sulfite in water where the ions are generally present to some degree.

Sulfite Detection in Wine

Encouraged by the results from above, and to extend the idea of sulfite detection in the food industry, we decided to test the ability of **OXJUL** to identify sulfite contained in a wine. To verify the reliability of the results the classic iodometric method was also performed (see ESI). A popular dry white wine was purchased from a local supermarket and an aliquot (0.5mL) was added to an EtOH/water mixture containing **OXJUL** and the fluorescence monitored over time. Under the conditions there was slight shift of the short wavelength profile to 590 nm, but the ratio changes were still observed and plateaued after about 8-10 mins. The results from three separate determinations are collected in Table 4, and for comparison are the results from experiments using the iodometry method. The agreement between the two methods is good indicating an average sulfite concentration of 0.63 mM (40 ppm). Sulfite concentrations in dry wine vary but are generally in the range 30-90 ppm;[27] the results from the fluorescence method are clearly viable.

Table 4. Calculated sulfite concentrations in a dry white wine using the fluorescence method and **OXJUL** compared to the standard iodometric method. The experiments were carried out in triplicate.

Run	OXJUL method		Iodometry method	
	Sulfite (mM)	Sulfite[a] (ppm)	Sulfite (mM)	Sulfite[a] (ppm)
1	0.59	38	0.62	40
2	0.66	42	0.65	42
3	0.63	40	0.57	37

[a] Calculated as SO_2 content.

Conclusions

Oxidation of the julolidine subunit appears to be feasible in the presence of silver ions and light when it is incorporated into a chromophore (i.e., **JUL**) displaying strong ground-state charge transfer. The general applicability of the method is yet to be fully tested, and it may be the vinylpyridine moiety is essential as a site for silver ion binding. A preliminary reaction using the vinylphenyl analogue of **JUL** showed very little sign of reaction under identical conditions used in the preparation of **OXJUL**.

Two distinctly different chemical reactions appear to occur when the sulfite anion is added to **OXJUL**. The first reaction is localised at the oxidised julolidine site which removes a double-bond from the ring. In the ground state the oxidised julolidine group is twisted with respect to the BODIPY core, but becomes more planar and π-conjugated in the excited state. The first hypsochromic shift in the fluorescence profile suggests the emissive state is less π-conjugated, which can be explained by the loss of the single double bond. In addition, there may also be an increase in the HOMO-LUMO gap because of an alteration in the electron withdrawing capacity of the oxidised julolidine. The much larger second hypsochromic shift is the result of a major perturbation of the BODIPY chromophore at the pyrrole group. The sulfite anion addition at this site completely disrupts the π-conjugation in the compound. Because of the two distinct sites for sulfite addition to **OXJUL** it does offer improved temporal sensing of the anion. In many other dye-based systems once the response is saturated, because all the dye is consumed, any additional sulfite cannot be detected. For **OXJUL** a long-term exposure to sulfite would induce the second fluorescence response and a new output signal.

Experimental

Material and Instrumentation

^{1}H-, ^{13}C- and DEPT-135° NMR spectra, as well as two-dimensional homo- (^{1}H/^{1}H COSY-45°) and heteronuclear (^{1}H/^{13}C HMQC and HMBC) correlation spectra were recorded with a Jeol ECS 400 MHz and a Bruker 700 MHz spectrometers. Chemical shifts for ^{1}H- and ^{13}C-NMR spectra are referenced relative to the residual protiated solvent. ^{11}B-NMR spectra are referenced relative to $BF_3{\cdot}OEt_2$. ^{19}F-NMR spectra are referenced relative to $CFCl_3$. Electronic absorption spectra were recorded at RT using a Shimadzu UV-1800 spectrophotometer. Fluorescence emission spectra were acquired at RT with Shimadzu RF-6000 fluorimeter.

X-Ray Crystallography

Crystal structure data for **OXJUL** were collected at 150 K on an Xcalibur, Atlas, Gemini Ultra diffractometer equipped with an Enhance Ultra (Cu) X-ray Source ($\lambda_{CuK\alpha}$ = 1.54184 Å) and an Oxford Cryosystems CryostreamPlus open-flow N_2 cooling device. Cell refinement, data collection and data reduction were undertaken via the CrysAlisPro[28] software. Intensities were corrected for absorption empirically using spherical harmonics. The structures were solved using XT[29] and refined using XL[30] through the Olex2 interface.[31] All non-hydrogen atoms were refined with anisotropic displacements and hydrogen atoms were positioned with idealised geometry and constrained using a riding model with the exception of those bound to heteroatoms in which case the positions of the hydrogen atoms were located using peaks in the Fourier difference map. The structure is deposited in the Cambridge Structural Database (CCDC 1909479).

Computational Modeling

In order to estimate the energies of BODIPY based and CT absorptions the spectrum profile in the red region was deconvoluted into four peaks with the PeakFit software. Three peaks were set to have the same full-width at half-maximum while the width of the fourth peak modelling the CT band was left independent. The fitted CT band was always about four times broader than the BODIPY-based transitions.

Energy-minimised structures of **JUL** and **OXJUL** were calculated in Gaussian 09[32] in order to describe and compare the frontier molecular orbitals. Firstly, the structures were optimised with the DFT B3LYP/3-21G method and the results were used as the input for calculations at the B3LYP/6-311+G(d, p), theoretical levels without any symmetry constraint in the gas phase. The optimised geometries were further used as input for calculations in DMSO solvent using IEF-PCM solvation model and the same theoretical level. The UV-Vis-NIR absorption spectra of the compounds in DMSO were calculated using IEF-PCM solvent model at B3PW91/6-311+G(d,p) TD-DFT theory level, and their images were obtained by using 0.1 and 0.2 eV half-widths at half-height for the BODIPY and CT transitions, respectively.

Fluorescence Sensing of SO_3^{2-}

A series of $NaSO_3$ solutions (1.3×10^{-6} - 1.3×10^{-2} mmol) were prepared in EtOH aqueous solution (75 %, v/v) to obtain a calibration plot. All solutions were excited at 525 nm. Fluorescence emission changes from 535 nm to 900 nm were measured to see the ratiometric change between 580 nm and

634 nm every 2 min until one hour. The sensing limitation was determined by 3σ/slope.[33] To test the selectivity of **OXJUL**, other anions F^-, Cl^-, Br^-, I^-, SO_4^{2-}, PO_4^{3-}, NO_3^-, NO_2^-, CO_3^{2-} and CH_3COO^- (3.9×10^{-4} mmol) were measured under the same conditions.

Real Sample Testing

A dry white wine (13% alcohol) purchased from local super market were diluted with an EtOH/aqueous solution respectively to give a EtOH-wine-aqueous mixture (3 mL, 75 % alcohol, v/v). Fluorescence emission changes from 535 nm to 900 nm were recorded every 20 seconds until 30 min. The value of sulfite in the real wine sample can be calculated through the calibration curve obtained above.

Independent measurement[34]

The iodometric method was used to determine the amount of sulfite in wine independently. A calibration plot was determined as per the validated stabilization procedure. A series of sulfite solutions with different concentration were titrated with a I_2 solution. A few drops of starch solution were added as indicator. The blue resultant solution was stabilized for 2 mins and then absorption spectra were measured in the 300 to 1100 nm region.

Wine samples (10 mL) were treated with NaOH solution (1.6 mL, 4 M) and H_2SO_4 (1.7 mL, 10% v/v) prior to the titration. A known amount of wine sample (< 5 mL) was added to a titrated I_2 solution (0.5 mL) in a vial containing an EtOH/aqueous solution and a few drops of starch indicator. The resultant blue solution was stabilized for 2 mins before recording UV-Vis absorbance spectra, and compared to the calibration curve to determine the sulfite concentration in the wine sample.

Synthesis

All chemicals were purchased from commercial sources and used as received unless otherwise stated. Basic solvents for synthesis were dried using typical literature methods. Solvents for spectroscopic investigations were of the highest purity available. The starting material **JUL** was prepared by using the method previously reported by our group.[16]

Preparation of OXJUL

Compound **JUL** (8 mg, 0.014 mmol, 1 eq) and silver trifluoromethanesulfonate (28.9 mg, 0.112 mmol, 8 eq) were dissolved in acetone (160 mL). The resulting mixture was irradiated by white LED light until the complete consumption of the starting material (7-10 days). The solution was filtered and most of the solvent was removed to precipitate a dark blue solid which was collected by centrifugation and dried under high vacuum (4 mg, 0.007 mmol, 50 % yield). ^{1}H-NMR (700 MHz, DMSO-d_6) δ (ppm) = 9.49 (d, *J* = 6.0 Hz, 1H, julolidine), 9.31 (d, *J* = 8.5 Hz, 1H, julolidine), 8.70 (br s, 4H, pyridine), 8.64 (d, *J* = 1.7 Hz, 1H, julolidine), 8.31 (d, *J* = 1.7 Hz, 1H, julolidine), 8.26 (dd, *J* = 8.5, 6.0 Hz, 1H, julolidine), 7.82 (s, 4H, CH=CH), 7.61 (d, *J* = 5.8 Hz, 4H, pyridine), 7.46 (d, *J* = 4.6 Hz, 2H, β-pyrrole), 7.11 (d, *J* = 4.6 Hz, 2H, β-pyrrole), 5.02 (t, 2H, julolidine), 3.39 (t, *J* = 5.8 Hz, overlapping with residual water, julolidine), 2.44-2.39 (m, overlapping with residual DMSO, julolidine). ^{13}C-NMR {HMBC} (176 MHz, DMSO-d_6) δ (ppm) = 154.41, 150.62, 149.49, 147.57, 142.69, 137.73, 136.09, 136.05, 135.98, 134.75, 131.07, 131.03, 129.90, 129.25, 122.37, 121.72, 121.60, 121.19, 118.98, 56.64, 26.33, 20.15. ^{11}B-NMR (96 MHz, DMSO-d_6) δ (ppm) = 1.16 (t, *J* = 33.0 Hz). ^{19}F-NMR (282 MHz, DMSO-d_6) δ (ppm) = -77.75 (s, $CF_3SO_3^-$) -136.75 (q, *J* = 33.4 Hz, BF_2).

Acknowledgements

We thank the Leverhulme Trust and Newcastle University for financial support. The National Mass Spectrometry Facility at Swansea University is also thanked for collecting mass spectra of the compounds.

Notes and references

1 a) M. Alkondon, A. C. Costa, V. Radhakrishnan, R. S. Aronstam and E. X. Albuquerque, *FEBS Lett.*, 1990, **261**, 124-130; b) M. Li, H. Gou, I. Al-Ogaidi, and N. Wu, *ACS Sustain. Chem. Eng.*, 2013, **1**, 713–723; c) S. Kolemen and E. U. Akkaya, *Coord. Chem. Rev.*, 2018, **354**, 121-134; d) X. Chen, G. Zhou, S. Mao and J. Chen, *Environ. Sci. Nano.*, 2018, **5**, 837-862.

2 a) A. Renzoni, F. Zino and E. Franchi, *Environ. Res.*, 1998, **77**, 68-72; b) A. Simpson, R. R. Pandey, C. C. Chusuei, K. Ghosh, R. Patel and A. K. Wanekaya, *Carbon*, 2018, **127**, 122-130; c) B. Cheng, L. Zhou, L. Lu, J. Liu, X. Dong, F. Xi and P. Chen, *Sensor. Actuat. B-Chem.*, 2018, **259**, 364-371.

3 a) K. Y. Goud, S. K. Kalisa, V. Kumar, Y. F. Tsang, S. Lee, K. V. Gobi and K. H. Kim, *Biosensors and Bioelectronics*, 2018, **121**, 205-222; b) R. D. Rocklin and E. L. Johnson, *Anal. Chem.*, 1983, **55**, 4-7; c) A. Ainla, M. P. Mousavi, M. N. Tsaloglou, J. Redston, J. G. Bell, M. T. Fernández-Abedul and G. M. Whitesides, *Anal. Chem.*, 2018, **90**, 6240–6246; d) A.C. Benniston, D. Sirbu, C. Turta, M.R. Probert, W. Clegg, *Eur. J. Inorg. Chem.*, 2014, **36**, 6212–6219.

4 a) C. F. Poole, *J. Chromatogr. A*, 2004, **1037**, 49-82; b) J. Yin, Y. Hu and J. Yoon, *Chem. Soc. Rev.*, 2015, **44**, 4619-4644; c) J. Hai, T. Li, J. Su, W. Liu, Y. Ju, B. Wang and Y. Hou, *Angew. Chem. Int. Edit.*, 2018, **57**, 6786-6790.

5 a) J. Zhai, X. Xie, T. Cherubini, and E. Bakker, *ACS Sens.,* 2017, **2**, 606–612; b) K. Thajee, L. Wang, K. Grudpan and E. Bakker, *Anal. Chim. Acta*, 2018, **1029**, 37-43.

6 a) E. Ritz, K. Hahn, M. Ketteler, M. K. Kuhlmann and J. Mann, *Dtsch. Arztebl. Int.* , 2012, **109**, 49-55; b) C. Storer, Z. Coldrick, D. Tate, J. Donoghue and B. Grieve, *Sensors*, 2018, **18**, 531.

7 a) R. Michalski, M. Jablonska and S. Szopa, *Crit. Rev. Anal. Chem.*, 2011, **41**, 133-150; b) J. Asselin, M. P. Lambert, N. Fontaine and D. Boudreau, *Chem. Commun.*, 2017, **53**, 755-758.

8 a) N. P. Sen and B. Donaldson, *J. Assoc. Off. Anal. Chem.*, 1978, **61**, 1389-1394; b) M. Cuartero, G. A. Crespo and E. Bakker,. *Anal. Chem.*, 2015, **87**, 8084-8089.

9 a) Q. Zhang, J. Zhang, H. Zuo, C. Wang and Y. Shen, *Tetrahedron*, 2016, **72**, 1244-1248.; b) C. Cheng, H. Y. Chen, C. S. Wu, J. S. Meena, T. Simon and F. H. Ko, *Sens. Actuat. B-Chem.*, 2016, **227**, 283-290.

10 A. Ghorai, J. Mondal, R. Chandra and G. K. Patra, *RSC Advances*, 2016, **6**, 72185-72192.

11 V. K. Gupta, N. Mergu, L. K. Kumawat and A. K. Singh, *Talanta*, 2015, **144**, 80-89.

12 M. R. Lester, *J. Am. Coll. Nutr.*, 1995, **14**, 229-232; b) C. Rueda, P. A. Calvo, G. Moncalián, G. Ruiz and A. Coz, *J. Chem. Tech. Biotech.*, 2015, **90**, 2218-2226.

13 a) D. Lowinsohn and M. Bertotti, *Food Addit. Contam. A*, 2001, **18**, 773-777. b) T. R. Dadamos and M. F. Teixeira, *Electrochim. Acta*, 2009, **54**, 4552-4558; c) K. S. Carlos and L. S. de Jager, *J. AOAC Int.*, 2017, **100**, 1785-1794.

14 a) C. Yu, M. Luo, F. Zeng and S. Wu, *Anal. Methods*, 2012, **4**, 2638-2640. b) X. Gu, C. Liu, Y. C. Zhu and Y. Z. Zhu, *J. Agric. Food Chem.*, 2011, **59**, 11935-11939; c) T. Gao, C. Xiaozheng, G. Peng, D. Jie, Y. Shuqi, X. Huan, W. Yong, G. Feng and Z. Wenbin, *Org. Biomol. Chem.*, 2017, **15**, 4375-4382.

15 a) V. R. Holland and B. C. Saunders, *Tetrahedron*, 1971, **27**, 2851-2854; b) X. Zeming, G. Xiaoyu, Z. Yanpeng, W. Yonggen and W. Jiaobing, *RSC Adv.*, 2018, **8**, 13588-13591.

16 a) D. Sirbu, J. B. Butcher, P. G. Waddell, P. Andras and A. C. Benniston, *Chem.-Eur. J.*, 2017, **23**, 14639-14649; b) D. Sirbu, S. Luli, J. Leslie, F. Oakley and A. C. Benniston, *ChemMedChem*, 2019, .

17 D. Bai, A. C. Benniston, S. Clift, U. Baisch, J. Steyn, N. Everitt and P. Andras, *J. Mol. Struct.,* 2014, **1065-1066**, 10-15.

18 a) G. Ulrich, R. Ziessel and A. Harriman, *Angew. Chem. Int. Ed.,* 2008, **47**, 1184-1201; b) D. Sirbu, A. C. Benniston, A. Harriman, *Organic Lett.*, 2017, **19**, 1626–1629; c) N. O. Didukh, Y. V. Zatsikha, G. T. Rohde, T. Blesener, V. P. Yakubovskyi, Y. P. Kovtun and V. N. Nemykin, *Chem. Commun*., 2016, **52**, 11563-11566.

19 a) P. G. Seybold and M. Gouterman, *J. Mol. Spectrosc.*, 1969, **31**, 1. b) J. K. G. Karlsson, O. J. Woodford, H. Mustroph and A. Harriman, *Photochem. Photobiol*. *Sci.,* 2018, **17**, 99-106.

20 J. Clayden, N. Greeves and S. Warren, Organic Chemistry, 2nd Edition, pp 138-139, Oxford University Press.

21 I. H. A. Badr, A. Plata, P. Molina, M. Alajarín, A. Vidal and L. G. Bachas, *Anal. Chim. Acta*, 1999, **388**, 63-69.

22 An NMR sample in d_6-DMSO containing Na_2SO_3 (aq) left for one week also showed signs of reaction at the dipyrromethene site by removal of the proton assigned to the β pyrrole. A small trace of acid furthermore resulted in the reappearance of protons associated with the cationic julolidine group (see ESI). It is noted that sulfite addition to the double bond may be reversible and acid addition after one week may simply result in protonation of reformed starting material. A ^{1}H NMR spectrum collected of **OXJUL** in d_6-DMSO after the addition of acid showed a severe broadening of peaks, but certain resonances were missing when compared to the spectrum left for a week with acid present (see ESI).

23 The species present in water depends on pH with $SO_2.H_2O$ dominating in acidic conditions (< 2) and HSO_3^- in the range 3-7. At high pH the SO_3^- ion is mainly present.

24 a) X. Pei, H. Tian, W. Zhang, A. M. Brouwer and J. Qian, *Analyst,* 2014, **139**, 5290-5296. b) Y. Zhu, W. Du, M. Zhang, Y. Xu, L. Song, Q. Zhang, X. Tian, H. Zhou, Y. Wu and Y. Tian, *J. Chem. Mat. Chem. B*, 2017, **5**, 3862-3869.

25 The Eigen-Wilkins mechanism for anion substitution within an octahedral geometry is a classic reaction displaying the same kinetic model.

26 For examples of other LODs see: a) S. Chen, C. Ma, M.-S. Yuan, W. Wang, D.-E. Wang, S.-W. Chen and Y. Wang, *RSC Advances*, 2016, **6**, 85529-85537. b) Q. Zhang, Y. Zhang, S. Ding, H. Zhang and G. Feng, *Sens. Actua. B-Chem*., 2015, **211**, 377-384. c) H. Zhang, S. Xue and G. Feng, *Sens. Actua. B-Chem*., 2016, **231**, 752-758.

27 J. W. Buechsenstein and C. S. Ough, *Am. J. Enol. Vitic.*, 1978, **29**, 161-164.

28 CrysAlisPro, Agilent Technologies, Version 1.171.36.32.

29 G. M. *Sheldrick, Acta Crystallogr. Sect. A,* 2015, **71**, 3–8.

30 G. M. *Sheldrick, Acta Crystallogr. Sect. A,* 2008, **64,** 112.

31 O. V. Dolomanov, L. J. Bourhis, R. J. Gildea, J. A. K. Howard, H. Puschmann, *J. Appl. Crystallogr.* 2009, **42,** 339.

32 Gaussian 09, Revision D.01, M. J. Frisch, G. W. Trucks, H. B. Schlegel, G. E.Scuseria, M. A. Robb, J. R. Cheeseman, G. Scalmani, V. Barone, B. Mennucci G. A. Petersson, H. Nakatsuji, M. Caricato, X. Li, H. P. Hratchian, A. F. Izmaylov, J. Bloino, G. Zheng, J. L. Sonnenberg, M. Hada, M. Ehara, K. Toyota, R. Fukuda, J. Hasegawa, M. Ishida, T. Nakajima, Y. Honda, O. Kitao, H. Nakai, T. Vreven, J. A. Montgomery, Jr. , J. E. Peralta, F. Ogliaro, M. Bearpark, J. J. Heyd, E. Brothers, K. N. Kudin, V. N. Staroverov, T. Keith,R. Kobayashi, J. Normand, K. Raghavachari, A. Rendell, J. C. Burant, S. S. Iyengar, J. Tomasi, M. Cossi, N. Rega, J. M. Millam, M. Klene, J. E. Knox, J. B. Cross, V. Bakken, C. Adamo, J. Jaramillo, R. Gomperts, R. E. Stratmann, O. Yazyev, A. J. Austin, R. Cammi, C. Pomelli, J. W. Ochterski, R. L. Martin, K. Morokuma, V. G. Zakrzewski, G. A. Voth, P. Salvador, J. J. Dannenberg, S. Dapprich, A. D. Daniels, O. Farkas, J. B. Foresman, J. V. Ortiz, J. Cioslowski, and D. J. Fox, Gaussian, Inc., Wallingford CT, 2013.

33 Y. Chen, C. Zhu, Z. Yang, J. Chen, Y. He, Y. Jiao, W. He, L. Qiu, J. Cen and Z. Guo, *Angew. Chem. Int. Ed.*, 2013, **52**, 1688-1691.

34 P. Musagala, H. Ssekaalo, J. Mbabazi and M. Ntale, *J. Toxicol. Environ. Health Sci.*, 2013, **5**, 66-72.